Available online at www.sciencedirect.com
SCIENCE DIRECT®
Physica A 327 (2003) 49–53
PHYSICA A
www.elsevier.com/locate/physa

Tracer dispersion of non-Newtonian fluids in a Hele–Shaw cell

A. Boschan[a,*], V.J. Charette[a], S. Gabbanelli[b], I. Ippolito[a], R. Chertcoff[a]

[a] *Grupo de Medios Porosos, Facultad Ingeniería, Universidad de Buenos Aires, Paseo Colón 850, 1063, Buenos Aires, Argentina*
[b] *Depto. de Matemática, Facultad Ingeniería, Universidad de Buenos Aires, Paseo Colón 850, 1063, Buenos Aires, Argentina*

Abstract

We report here a study of the transport and tracer dispersion properties of fluids in a model of fractured media. The tracer dispersion process was analyzed using Newtonian and non-Newtonian fluids (polymeric solutions). Experiments were carried out in a Hele–Shaw cell using axial flow and dyes as tracers. We analyze the influence of polymers presenting shear-thinning characteristics on the dispersion properties. It was found that the dispersion coefficient decreases when polymer concentration increases.

PACS: 47.50.+d; 83.10.Ji; 05.60.+w

Keywords: Dispersion; Fracture; Non-Newtonian

1. Introduction

Polymers are of interest in several applications such as oil recovery, chemical engineering and others [1]. The aim of this work is to study tracer dispersion for both Newtonian and non-Newtonian flows. We have used shear-thinning polymers, that, compared to Newtonian fluids, provide a higher contrast between large and small flow channels [2]. Tracer dispersion corresponds to the spreading of an initially localized tracer concentration distribution due to the combined effects of molecular diffusion and

* Corresponding author.
E-mail address: abosch@fi.uba.ar (A. Boschan).

0378-4371/03/$ - see front matter © 2003 Published by Elsevier B.V.
doi:10.1016/S0378-4371(03)00437-0

the velocity field of the flow. In homogeneous systems, the variation of the tracer concentration C satisfies the classical macroscopic advection–diffusion equation [3]:

$$\frac{\partial C}{\partial t} + U\frac{\partial C}{\partial x} = K_g \frac{\partial^2 C}{\partial x^2}\,, \tag{1}$$

where U is the mean flow velocity and K_g the longitudinal dispersion coefficient (where we have neglected the transverse dispersion). For $x = L$ (L is the size of the sample) the solution of Eq. (1) is

$$C(L,t) = \frac{1}{2}\left[1 - erf\left(\frac{L - Ut}{2\sqrt{K_g t}}\right)\right]\,. \tag{2}$$

Solution (2) corresponds to a "Gaussian" tracer dispersion. The variation of the longitudinal dispersion coefficient with the mean velocity for a flow between two parallel flat plates is [4]

$$K_g = D_m + \frac{d^2U^2}{210D_m}, \quad \frac{K_g}{D_m} = 1 + \frac{Pe^2}{210}\,, \tag{3}$$

where d is the distance between plates, and D_m is the molecular diffusion coefficient (a similar result was earlier found by Taylor–Aris [5] for a capillary tube). In the Newtonian case the velocity profile corresponds to Poiseuille flow while for non-Newtonian fluids the profile is "plug-like" [6]. In the last case, the coefficient of dispersion can be obtained analytically (A. Boschan, Tesis de Licenciatura en Fisica, FCEN, Universidad de Buenos Aires, 2002)

$$K_g = \frac{U^2d^2}{4D_m}\frac{n^2}{(n+1)^2}\left[\frac{1}{6} - \frac{n^2}{(3n+1)(4n+1)} - \frac{2n+1}{2(4n+1)} + \frac{(2n+1)n}{(3n+1)(5n+2)}\right], \tag{4}$$

where n is the flow index of the fluid which characterizes the rheological properties. Replacing $n = 1$ in Eq. (4) we find Eq. (3).

2. Experimental setup

The Hele–Shaw cell was constructed using two rectangular and parallel flat glass plates (35 cm × 20 cm × 1 cm). Two mylard strips (35 cm × 4 cm × 0.0375 cm) that separate the plates ($d = 0.0375$ cm) are placed over the longest sides allowing to establish an axial flow in the cell (Fig. 1). The cell is mounted in an aluminum frame and sealed with silicone glue to avoid losses. Two 3-point acrylic distributors allow to inject (drain) the fluids. They are placed at the enter (injection) and the exit (drainage) of the cell. A CCD camera (Coolsnap CF, monochrome, 4095 gray levels) is placed at 1 m around on the top of the cell getting full view, while four fluorescent tubes provide required illumination through a white acrylic (2 mm-thick) light diffusor (Fig. 1). The aqueous solutions used during the experiments were glycerol 10% for the Newtonian experiments and xanthan (with different concentrations) for the non-Newtonian

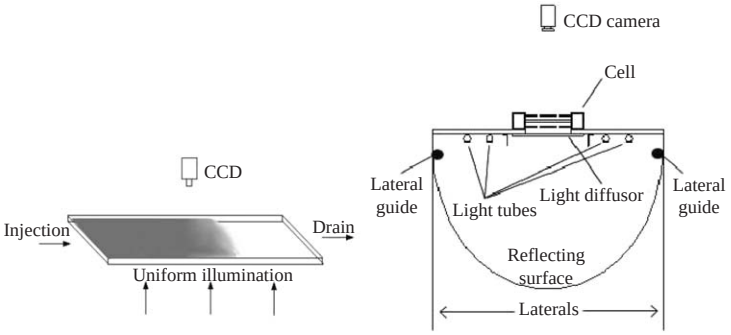

Fig. 1. Left: Hele–Shaw cell. The dyed fluid (tracer) displaces the transparent fluid while the camera captures the intensity variation in all the cells. Right: Scheme of the illumination system.

experiments. WaterBlue (0.4 g/l) was used as a tracer for both type of experiments to color the corresponding fluid. Densities were matched in all cases adding ClNa (0.4 g/l) to the transparent fluid in order to avoid gravity-driven instabilities. For each experience the cell is first filled with transparent fluid. Then the distributor chamber is filled with colored fluid (step-like initial condition for the tracer concentration). An experiment begins when the tracer is pumped at constant flow rate while the camera acquires images at a fixed time interval (given by a digital timer) proportional to the experiment duration. The mixing zone advances while it spreads from the enter (injection distributor) to the exit of the cell. The acquisition ends when the mixing zone reaches the exit. Flow rate was varied from 0.072 to 3.6 cm^3/seg, and the corresponding *Pe* values were between 50 and 2500. The viscosity of the polymeric solutions used in our experiments decreases with the shear rate (shear-thinning characteristic) except for very high or low shear rates, where the viscosity is constant. The behavior in the intermediate zone can be described with the power law model $\mu = k\dot{\gamma}^{n-1}$; where n is the flow index, μ is the viscosity, k is the consistence of the fluid and $\dot{\gamma}$ the shear rate. We have characterized the rheological behavior of the two polymeric solutions used, obtaining flow indexes $n = 0.55$ and 0.65 for the highest and lowest concentrations, respectively.

3. Image processing and data analysis

For each experiment we obtain a time sequence of 250 images (1330×650 pixels) which are stored in a multilayer TiFF file. The time interval between images varies from 1 to 60 s according to the flow rate. The variation between maximum and minimum gray-level value is approximately 1200. The gray level is proportional to the light intensity. To obtain the spatiotemporal intensity diagram we take a given longitudinal slice of the cell image and we examine the time evolution over the 250 images. The vertical axis in Fig. 2 represents this time variation. From this diagram the *intensity* vs. *time* curves were obtained for 20 longitudinal positions along the cell. A calibration of the tracer concentration and the intensity (or gray level) was performed and comparing

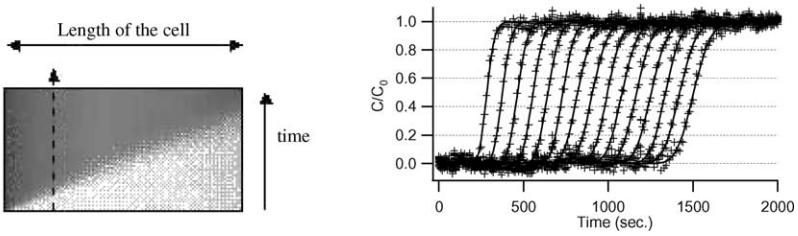

Fig. 2. Left: Spatiotemporal diagram. The dashed line shows how intensity curve is obtained for one longitudinal position in cell. Right: Concentration profiles for different positions along the cell ($Pe \approx 360$).

to the Lambert–Beer law, we have found a linear variation [7]. In this way we compute the curves of tracer concentration as a function of time (Fig. 2). The uniformity of the cell thickness was verified by measuring the intensity at different positions in the cell for a given concentration (the precision is given by the camera noise: 3%). These curves are well fitted by Eq. (2). From the fittings, we compute the mean transit time T_0 and the mean time square deviation of the distributions. For a given Pe number, in all experiments T_0 varies linearly with the measuring positions indicating that the mean flow velocity is constant. The mean square deviation is related to the coefficient of dispersion as follows [8]:

$$\overline{\Delta t^2} = 2\,\frac{K_g}{U^2}\,T_0\ . \tag{5}$$

Then, we calculate K_g from the slope of the curves $\overline{\Delta t^2}$ vs T_0 for each Pe value.

4. Experimental results

In Fig. 3, we have plotted the variation of K_g/D_m as a function of the Pe number for Newtonian ($n = 1$) and non-Newtonian fluids with $n = 0.55$ and 0.65.

The coefficient of dispersion has been normalized by molecular diffusion ($D_m = 2.4 \times 10^{-6}$ cm^2/s). Let us discuss first the variation of K_g/D_m for experiments performed with Newtonian solutions. We have superimposed prediction given by Eq. (3) as a reference. We can observe that the dimensionless dispersion coefficient increases quadratically with the Pe number according with Golay [4] and Taylor–Aris [5]. So we can say that this experimental technique represents an excellent tool to study tracer dispersion in this geometry. For the non-Newtonian fluids the dispersion coefficient also increases proportionally to Pe^2 for both n values. The analytical predictions for the non-Newtonian case, Eq. (4), are in quite good agreement with the experimental results. On the other hand, we can observe that the non-Newtonian K_g/D_m values are smaller than Newtonian ones. Even more, for a given Pe number, K_g/D_m decreases as the flow index n decreases. We think that this is due to the gradual flattening of the velocity profile (parabolic for Newtonian flow and plug-like profile for non-Newtonian flows) as the flow index decreases.

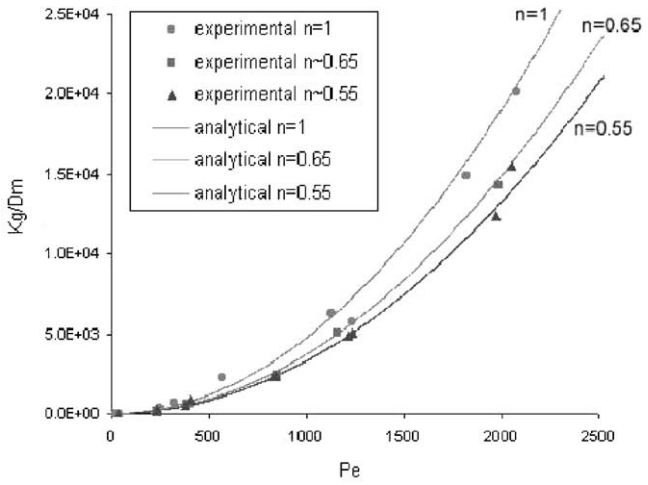

Fig. 3. Normalized coefficient of dispersion for Newtonian and non-Newtonian fluids. Only data points attaining Taylor regime are shown.

5. Conclusions

The developed experimental technique is very useful to characterize tracer dispersion. In all cases the dispersion coefficients for non-Newtonian fluids are smaller than for Newtonian ones. This behavior is contrary to what was observed in porous media: The dispersion coefficients in the non-Newtonian case are larger (shear-thinning fluids) than in the Newtonian case [2]. The difference is essentially due to the variations in the local velocities related to the geometry of the systems. In order to study that in more detail numerical simulations are in progress.

Acknowledgements

This work was partially supported by Fundación Antorchas, U.B.A PB-IO49 and the cooperation programs PICS CNRS 561 and ECOS_SUD E03-A97.

References

[1] F.A.L. Dullien, Porous Media, Fluids Transport and Pore Structure, Academic Press, New York, 1979.
[2] A. D'Onofrio, Ph.D. Thesis, Univ. de París VI, Univ. Buenos Aires, 2000.
[3] J. Bear, Dynamics of Fluids in Porous Media, American Elsevier, New York, 1972.
[4] M.J.E. Golay, in: D.H. Destye (Ed.), Gas Chromatography, Butterworths, London, 1958.
[5] R. Aris, On the dispersion of solute in a fluid flowing through a tube, Proc. Roy. Soc. London A 235, 67–77.
[6] K.S. Sorbie, Polymer-Improved Oil Recovery, Blackie, London, 1990.
[7] A. Boschan, Tesis de Licenciatura en Física, FCEN, Universidad de Buenos Aires, 2002.
[8] J. Koplik, Hydrodynamic dispersion in random networks, in: Disorder and Mixing, Serie E, Kluwer Academics Publishers, Dordrecht, 1987, pp. 107–122.